

Langley Grant
N-74-CR
198633
508

SIX MONTH REPORT
ON OPTICAL FIBER SENSORS AND SIGNAL PROCESSING
FOR INTELLIGENT STRUCTURE MONITORING

NASA GRANT NAG-1-895

DECEMBER 1988

Prepared for: Dr. Robert Rogowski
NASA Langley Research Center
Hampton VA 23665

Prepared by: Dr. R. O. Claus
Dr. D. K. Lindner
Daniel Thomas
Dave Cox
FEORC Virginia Tech
Blacksburg VA 24061

(NASA-CR-184841) OPTICAL FIBER SENSORS AND
SIGNAL PROCESSING FOR INTELLIGENT STRUCTURE
MONITORING Semiannual Report (NASA) 50 p
CSCL 20F

N89-21640

Unclas
G3/74 C198638

CONTENTS

Summary.....	1
1. Experimental Hardware	2
2. Analytical Analysis	5
3. Control Design.....	16
4. Sensor Development.....	23
References	25
Appendix A: August 1988 Report.....	26

Summary

This is the six-month summary report for NASA Grant NAG-1-895 titled "Optical Fiber Sensors and Signal Processing for Intelligent Structure Monitoring."

The major objective of this grant program is to investigate the analytical and experimental performance of optical fiber sensors for the control of vibration of large aerospace and other structures. In particular, modal domain optical fiber sensor systems, developed as part of prior NASA-supported research efforts at Virginia Tech, are being studied due to their apparent potential as distributed, low mass sensors of vibration over appropriate ranges of both low frequency and low amplitude displacements.

Progress during the past three months of this program is outlined in the beginning sections of this report; progress during the first three months of the program are discussed in Appendix A which formed a three-month report submitted in September 1988. Progress since September is divided here into work in the areas of experimental hardware development, analytical analysis, control design and sensor development. During the next six months, tests of a prototype closed-loop control system for a beam are planned which will demonstrate the solution of several optical fiber instrumentation device problems, the performance of the control system theory which incorporates the model of the modal domain sensor, and the potential for distributed control which this sensor approach offers. These tests are scheduled to begin prior to or during the Fiber & Electro-Optics Research Center's third annual review conference in late April 1989. The final report for this project is due in June 1989.

1. EXPERIMENTAL HARDWARE

MOTOR AND BEAM

All of the hardware required to perform the slewing beam experiment has been acquired. This includes a DC motor for actuation, a current amplifier, a flexible beam, digital and analog computers. The beam is instrumented with three strain gauges, which are located at the points of peak strain in the first three modes. These gauges feed bridge circuitry which generates a signal proportional to strain. The digital computer interfaces with the signals through A/D and D/A boards. Using a digital computer to execute the control law provides versatility and helps to fine tune the design through iteration. The computer also makes possible the acquisition and analysis of experimental data.

OPTICS

The first problem encountered in using the fiber optic strain sensor was one of modal stability. The dual mode fiber actually supports four linearly polarized modes, since each mode has even and odd degeneracies. The degenerate modes have the same propagation velocities, however, they have different spatial orientation with respect to the fiber endface. Under strain power is coupled into these degenerate modes. Since the first mode has a symmetric pattern it is unaffected by this coupling of power. The second mode, however, has a two lobe pattern which shifts its orientation when coupling occurs. This causes a distortion of the far field pattern, and

ultimately results in incorrect measurements of the induced strain.

Research carried out at Stanford University [1,2] suggested that an elliptical core fiber could prevent coupling into the degenerate modes. This occurs because a mode pattern orientated along the major axis of the ellipse will have a lower cutoff frequency that one orientated along the minor axis. A sample of elliptical core fiber was obtained from Andrew Corporation and tested in our labs. The fiber exhibited a stable two lobe pattern, and proved to be reliable under both static and dynamic strain tests [3]. The elliptical core fiber has a larger difference in index of refraction between the core and cladding than standard communication fiber. In communication applications this difference leads to modal dispersion, which causes pulse spreading and lowers bandwidth. In modal domain sensing, however, this dispersion is used to detect strain and as a result the elliptical core fiber is about three times as sensitive as circular core fiber.

The second problem encountered was one of instrumenting the beam with the fiber optic cable. The fiber senses strain along its entire length, therefore, the leads which go from the laser to the beam, and from the beam back to the photodetector will pick up extraneous strain. Since the beam is to be slewed these leads will move and introduce an unacceptable amount of noise into the sensor signal.

To solve this problem nonsensing leads were needed to carry light to and from the sensing section of two mode fiber. A single mode fiber was fused to the elliptical core fiber using an oxygen propane torch. The single mode fiber guides light from the laser to the two mode fiber, and the light's intensity is

not effected by small movements in the single mode fiber. Since the elliptical core fiber is polarization sensitive a shift in the polarization in the single mode fiber would cause a decrease in optical power at the output of the elliptical core fiber. To prevent this a high birefringent single mode lead must be used. Furthermore, the polarization preserving axis of the single mode fiber must be aligned with the major axis of the ellipse when the fibers are fused. Experiment verified the ability of light from a single mode fiber to excite two modes in the elliptical core fiber. In addition disturbances in the single mode lead did not seem to effect the output of the two mode fiber.

The task of removing the signal from the beam was less difficult. A large core fiber is to be placed in the far field pattern of the elliptical core fiber. This fiber serves as both a spatial filter of the output pattern, and as a waveguide to carry light back to the photodetector. Since this fiber carries amplitude information only, phase shifts due to extraneous strain will not effect its performance.

These nonsensing leads have been tested independently, however, a fully instrumented beam has not yet been created. Analysis has shown that the amount of fiber on the beam, and the path which it follows have significant effects on the system model. The optimal fiber placement is yet to be determined, and this has delayed the construction of a fully instrumented beam.

2. ANALYTICAL ANALYSIS

SYSTEM IDENTIFICATION

In order to efficiently design control schemes, a detailed and accurate model of the system must be developed. Towards this end much work has been done in the area of system identification. The DC motor being used as an actuator has the model:

$$\frac{\theta}{V} = \frac{K_t}{R_a J_m s^2 + K_t K_b s}$$

Where:

- θ = Position of shaft
- V = Applied voltage
- K_b = Back EMF constant
- K_t = Torque constant
- R_a = Armature resistance
- J_m = Armature Inertia

The back EMF constant was determined by back driving the motor. A second motor was connected to the actuator shaft through a flexible coupler. The actuator was back driven at various speeds and the voltage generated at the actuator terminals was recorded. This test provided consistent results at different speeds, and produced an accurate value for the back EMF constant. Since a DC motor can be operated as either a generator or a motor, the torque constant and the back EMF constant relate the same fundamental parameters. The constants are equal in value, but have different units. Therefore no further testing was necessary to determine the torque constant.

The armature resistance is a measure of resistance inherent in the

ORIGINAL PAGE IS
OF POOR QUALITY

armature windings. This term was simply measured with a digital voltmeter.

The armature inertia was not measured directly. This would require disassembling the motor to remove the armature windings from the effects of the stator's magnetic field. Instead, since this was the only parameter left to be determined, the motor's frequency response was tested and the transfer function was fit to match this response.

Two techniques were used to develop the motor's frequency response. The first involved driving the motor with sinusoids from a function generator. The input voltage and motor velocity were recorded on a strip chart. The ratio of velocity to input voltage was then used to generate a bode plot of the transfer function. The results of this test are shown in Figure 1, by the curve labeled "Frequency Test". Because it was difficult to generate a large number of data points and because of the limited accuracy of a strip chart recording, a second test was conducted.

The second test involved driving the motor with a wide band noise source. The source data was digitally generated and a FFT of the data showed that it possessed a relatively even distribution of power in the frequency range of interest. This data was output through an A/D board to the motor. With this noise driving the motor, data was collected from the tachometer and digitally stored. The input and output data was then processed via a FFT algorithm and the spectral densities were correlated to produce the frequency response of the motor. This response is also shown in Figure 1 by the curve labeled "Noise Test". This test gave a more accurate roll off at high frequencies.

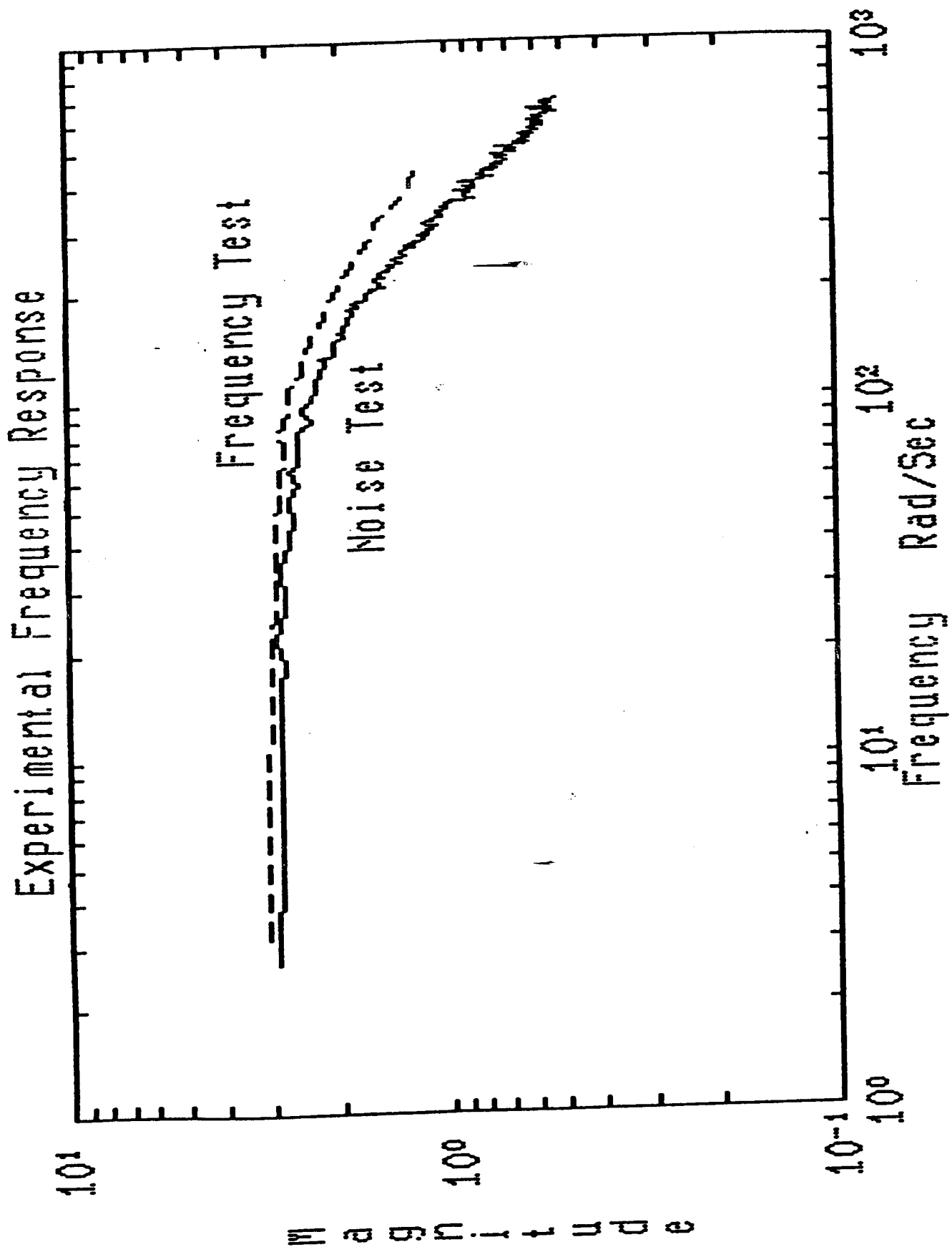


Figure 1

Therefore, the transfer function was fit to the noise test curve and a value was determined for the rotor inertia. With all of these parameters experimentally determined, the linear motor model was complete.

In order to include nonlinear effects in the system simulation, another simple motor test was performed. The motor was driven with a range of DC voltages and the velocity was recorded corresponding to each voltage. This data is shown in Figure 2. The motors deadband was set at 2.2 volts since no significant motion occurred at voltages below this level. The saturation was an abrupt cutoff since it was due to the amplifier and not the motor. The amplifier has negligible dynamics, therefore its gain and saturation characteristics are lumped together with the motor model.

The next step towards system identification was to test the parameters of the beam. The natural frequencies of a fixed free beam are given by:

$$\omega_n = B_n l^2 \sqrt{\frac{EI}{ml^4}}$$

Where:

- ω_n = frequency of the mode n
- B_n = coefficient of differential equation
- l = Length of beam
- E = Young's modulus
- I = Mass moment of inertia
- m = Mass of beam

The only term which required experimental verification was the product EI. The beam was instrumented with an optical fiber, which measured time varying strains along its length. The beam was then placed in a clamped free configuration, and disturbed such that the first few modes were excited. This

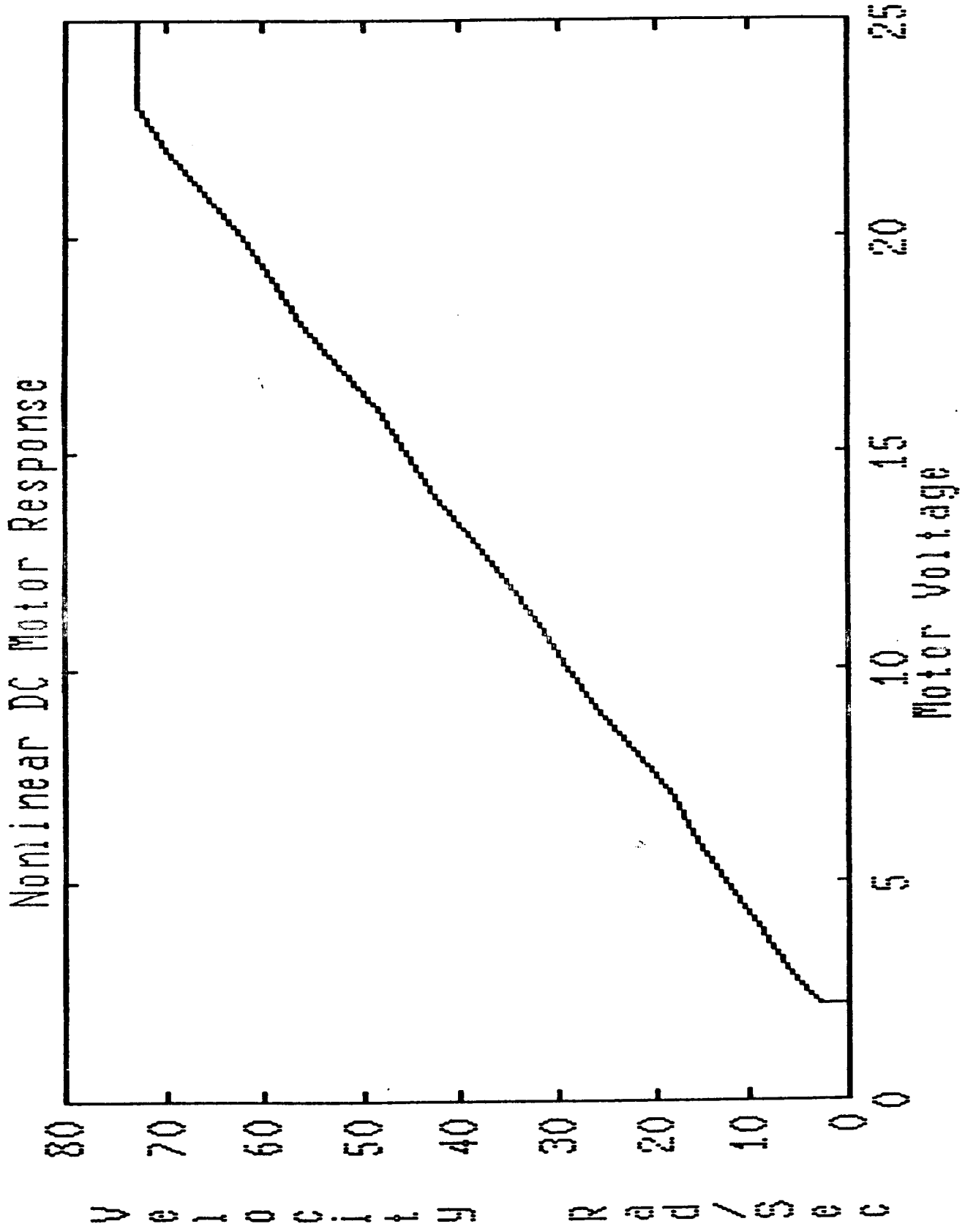


Figure 2

ORIGINAL PAGE IS
OF POOR QUALITY

information was stored in a digital oscilloscope and processed via a FFT algorithm. The beam's first three mode frequencies were apparent from the frequency spectrum. This information, along with the beam's mass and length allowed us to back calculate the EI term.

The table below gives the actual values for all of the experimentally determined system parameters.

$$K_t = .288 \text{ Nm/A}$$

$$K_b = .288 \text{ V/Sec}$$

$$R_e = 5.2 \text{ Ohms}$$

$$J_m = 0.00012 \text{ kgm}^2$$

$$EI = 0.44 \text{ Kg}^2\text{m/Sec}^2$$

All of this information was substituted into the original equations of motion in order to generate a state space model [A]. Some final adjustments to the model were made while in the state space form. The use of this model in simulations and comparisons, with the actual system, are the topics of the next section.

SIMULATION

The clamped flexible beam and actuator system has been modeled. The model was developed in the 3 month report [A]. A computer program has been generated to simulate the model. The program was developed in-house to obtain greater flexibility with the handling of nonlinearities in the system.

The simulation program utilizes a differential equation solver, which steps the model through time. The differential equation solver used is a subroutine of the International Mathematics Subroutine Library (IMSL). The subroutine uses the Runge-Kutta-Verner fifth order method. The model was put into the following system of first order differential equations for use by the program.

$$\dot{x} = Ax + BE_e$$

where

E_e = reference input voltage

x = state

$$A = \begin{pmatrix} 0 & I \\ -M^{-1}K & -M^{-1}D \end{pmatrix}$$

$$B = \begin{pmatrix} 0 \\ M^{-1}Q \end{pmatrix}$$

and M, D, K, and Q are the coefficient matrices developed in appendix A. The program was designed such that the number of modes the system is approximated with can be specified. The output consists of 6 data fields which are plotted with respect to time. These are the outputs of the 6 sensors, which are position, velocity, strain gauges 1-3, and the optical fiber. The actuator deadband and saturation nonlinearities are included in the simulation, and the optical fiber nonlinearities are currently being incorporated. This simulation will provide a useful tool in developing preliminary control designs for the optical fiber sensor and to observe how the modeled nonlinearities affect the design.

ORIGINAL PAGE IS
OF POOR QUALITY

In order to verify the system model it was necessary to compare the step responses of the actual system to those predicted by theory. Position and velocity feedback gains were chosen such that the motor would track a step input with a small rise time and little overshoot. With the beam fixed to the motor shaft a step was commanded and signals from the strain gauges, potentiometer and tachometer were digitally recorded. These signals represent the response of the system to a step input when no vibrational control is applied.

The simulated step response of the system model was also generated using the same position and velocity gains as above. Figures 3, 4, and 5 display the comparisons of position, root strain, and mid strain respectively. The simulated responses are accurate not only in the fundamental frequency of vibration, but also in the high frequency transient.

ORIGINAL PAGE IS
OF POOR QUALITY

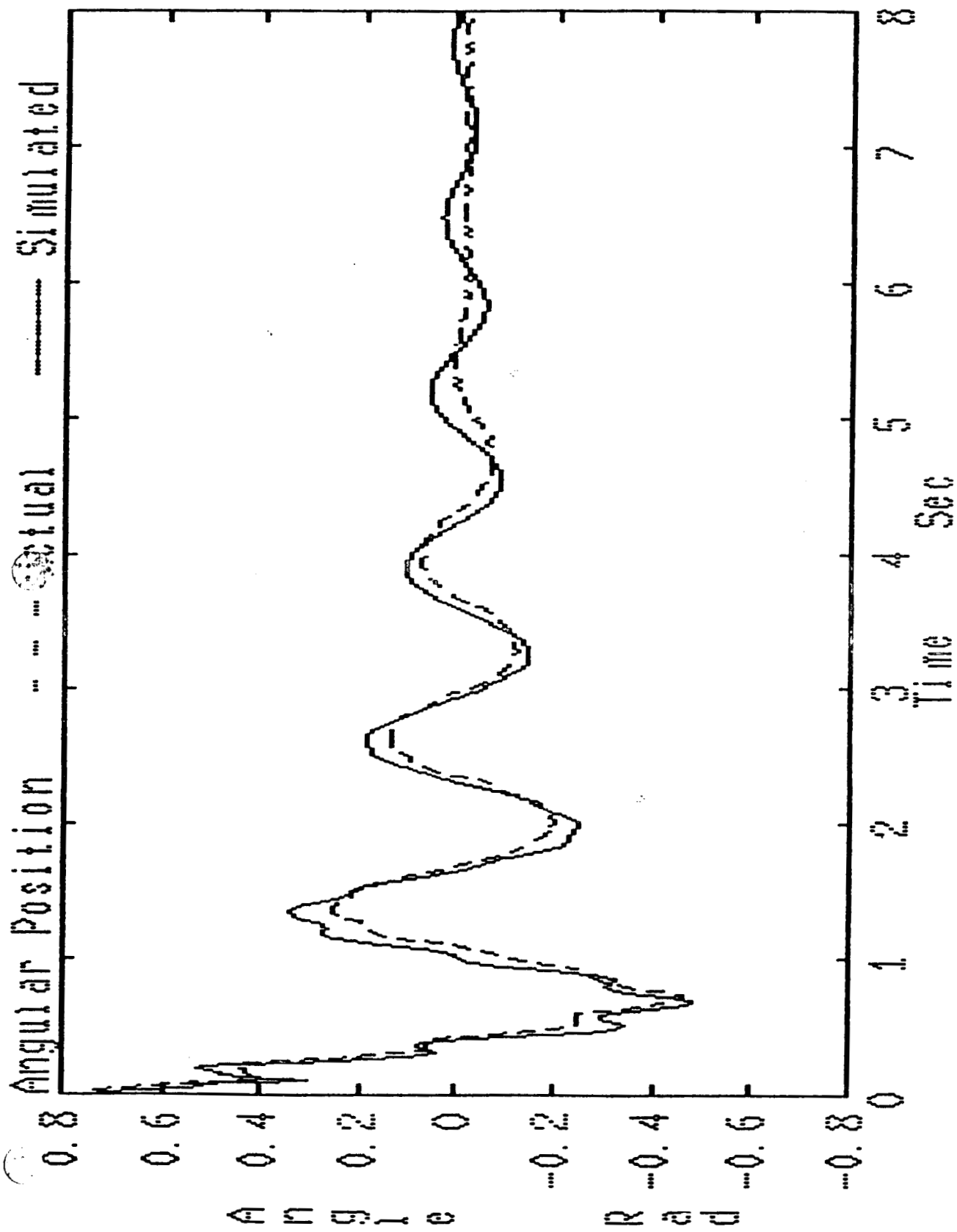


Figure 3

ORIGINAL PAGE IS
OF POOR QUALITY

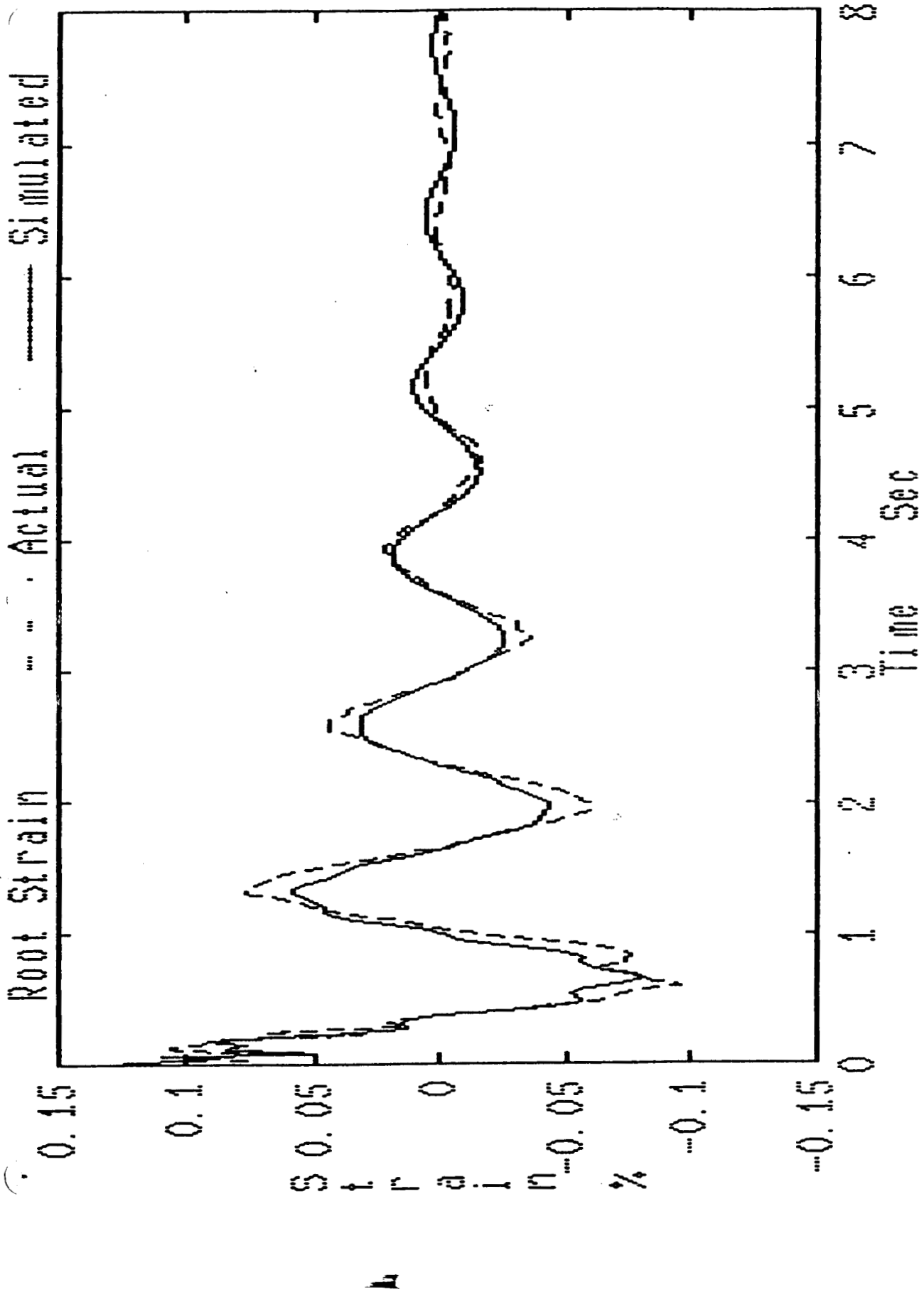


Figure 4
-14-

ORIGINAL PAGE IS
OF POOR QUALITY

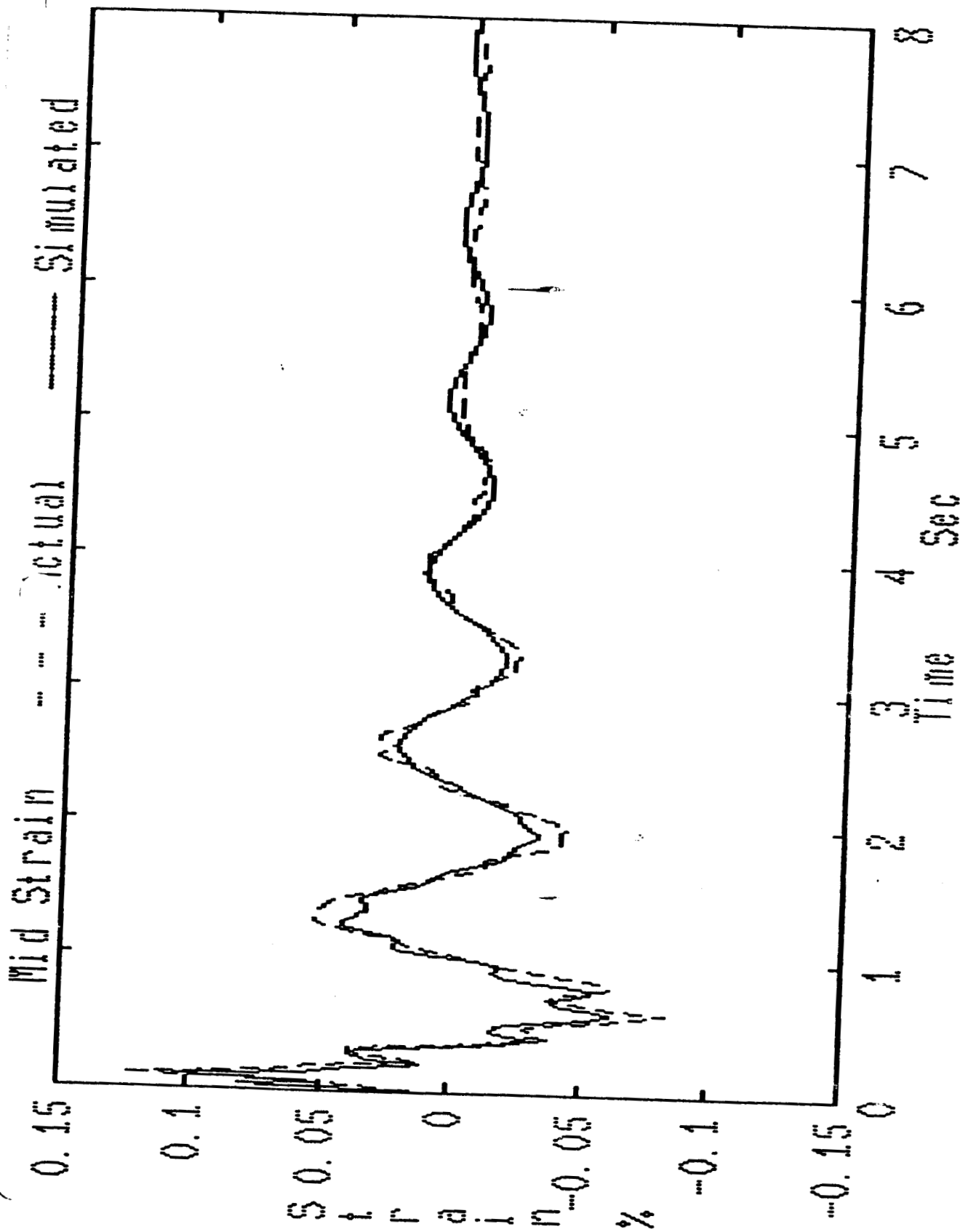


Figure 5

ORIGINAL PAGE IS
OF POOR QUALITY

3. CONTROL DESIGN

Using classical control theory techniques, we have developed a preliminary control system design for the flexible slewing beam with the optical fiber used as a sensor. The design employs 3 nested feedback loops. The inner-most loop is velocity gain feedback used to adjust the frequency response of the actuator. The middle loop uses angular position gain feedback to control pointing of the beam. This allows us to control the slewing of the beam. The outer loop employs optical fiber sensor compensated feedback to add damping to the flexible beam and control vibrations. The velocity and angular position feedback gains were obtained by considering reasonable rise time, overshoot, and practical gain limitations of the hardware. The rise time and overshoot criteria were not crucial since the objective is to damp vibrations out using the optical fiber sensor.

The root locus of the transfer function from the reference input to the output of the optical fiber for the 3 mode system appears in Figure 6. In the root locus plot, the X's represent the poles of the transfer function and the O's represent the zeros. As gain feedback is applied to the system, the poles move toward the zeros. If the trajectory the poles take enter into the right half plane, the system will be unstable for that range of gains. The objective of the preliminary control design is to alter the path of the second mode poles so that they do not enter the right half plane. If the poles can be moved

ORIGINAL PAGE IS
OF POOR QUALITY

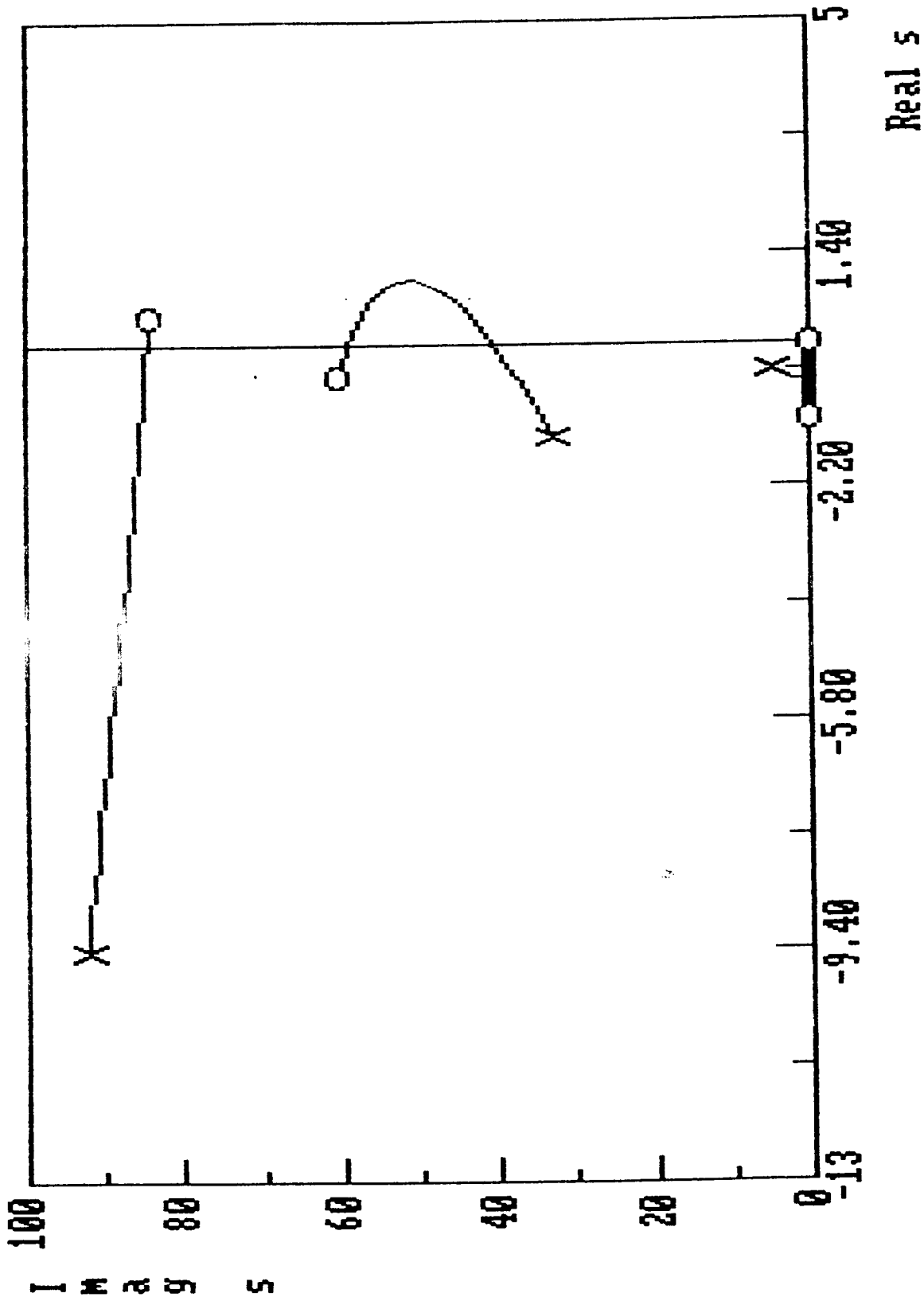


Figure 6: Root Loci of
Uncompensated 3 Mode Model

farther into the left half plane then the system will display more damping. The first cut assumption is that the first order poles retain enough inherent damping and the higher order poles are slow moving enough to neglect. A slow moving pole transverses slowly along it's trajectory with respect to the gain applied. The compensator must be made robust so that it will curb the path of the second order poles independent of which truncated modal model is used.

The design led us to the following second order lead compensator.

$$c(s) = \frac{(s+3)^2 + 20^2}{(s+4)^2 + 25^2}$$

The affect of the compensator on the third mode model can be seen in Figure 7. In this root locus, the second mode pole travels to the added zero. The trajectory break away angle of the pole is thus shifted 180 degrees to cause the pole's trajectory to lie in the left half plane. The closed loop time response of the optical fiber sensor output for the uncompensated system is shown in Figure 8 and the compensated system is shown in Figure 9. The compensated closed loop time response has a peak strain over 4.5 times less than that of the uncompensated system. The settling time has been reduced from 10.3 seconds to 5.8 seconds, where the settling time here is defined as the time required for the amplitude of the vibrations to drop below 0.13 microstrain.

Future work will be aimed at optimizing preliminary control designs. These designs will first be ~~tested~~ tested, as this one had been done, with the

ORIGINAL PAGE IS
OF POOR QUALITY

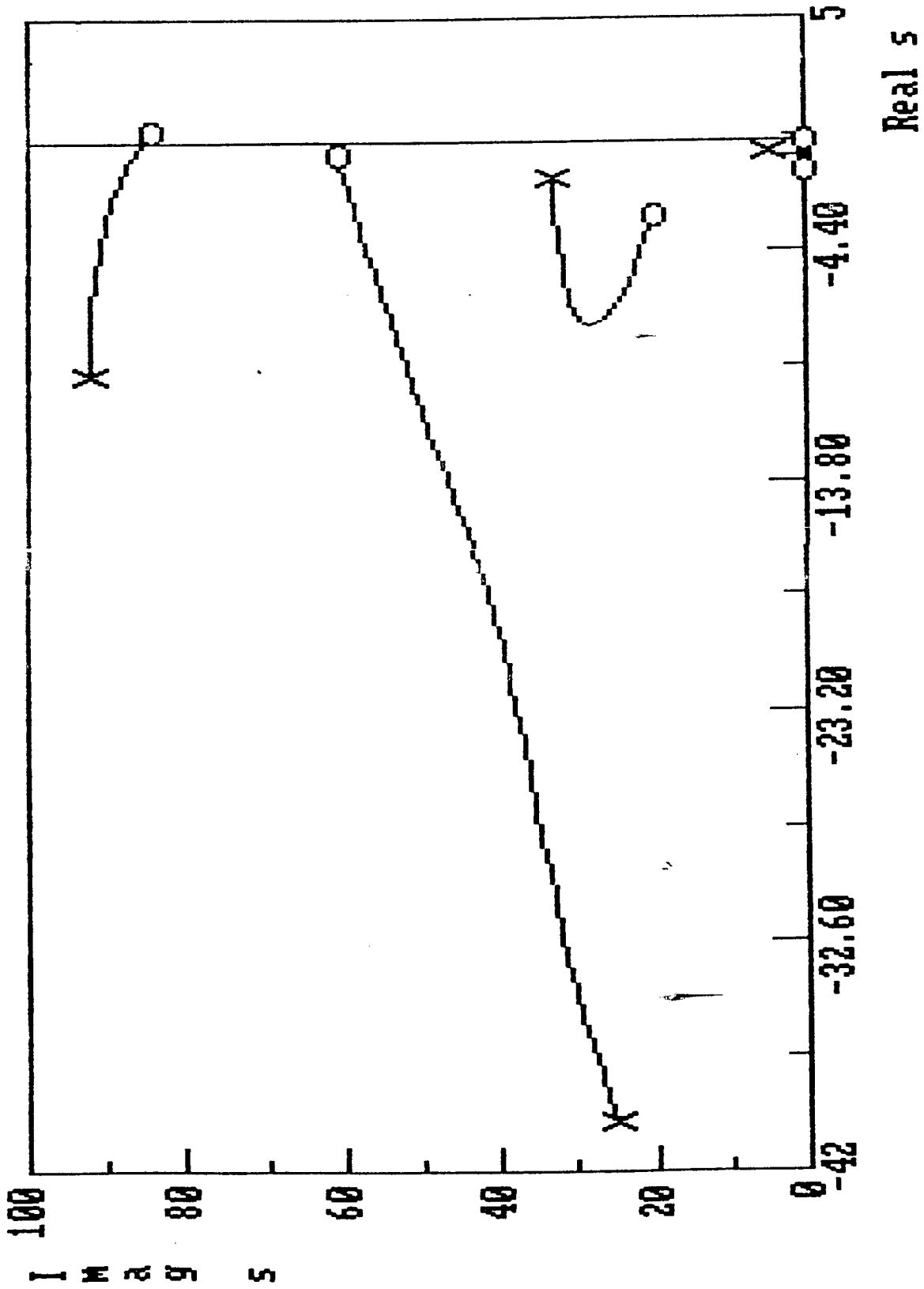


Figure 7: Root Loci of
Compensated 3 Mode Model

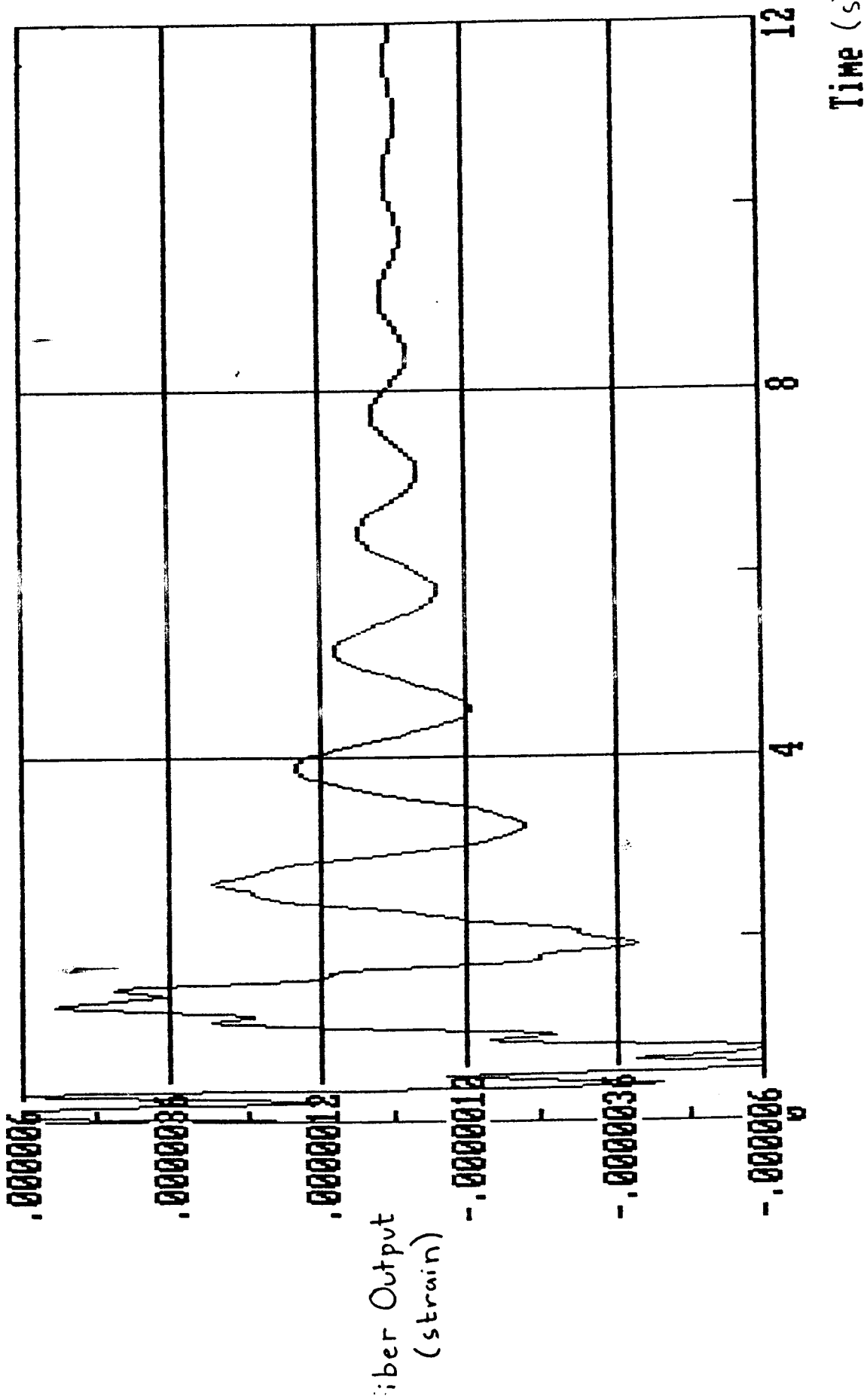


Figure 8: Optical Fiber Sensor
Time Response of Uncompensated

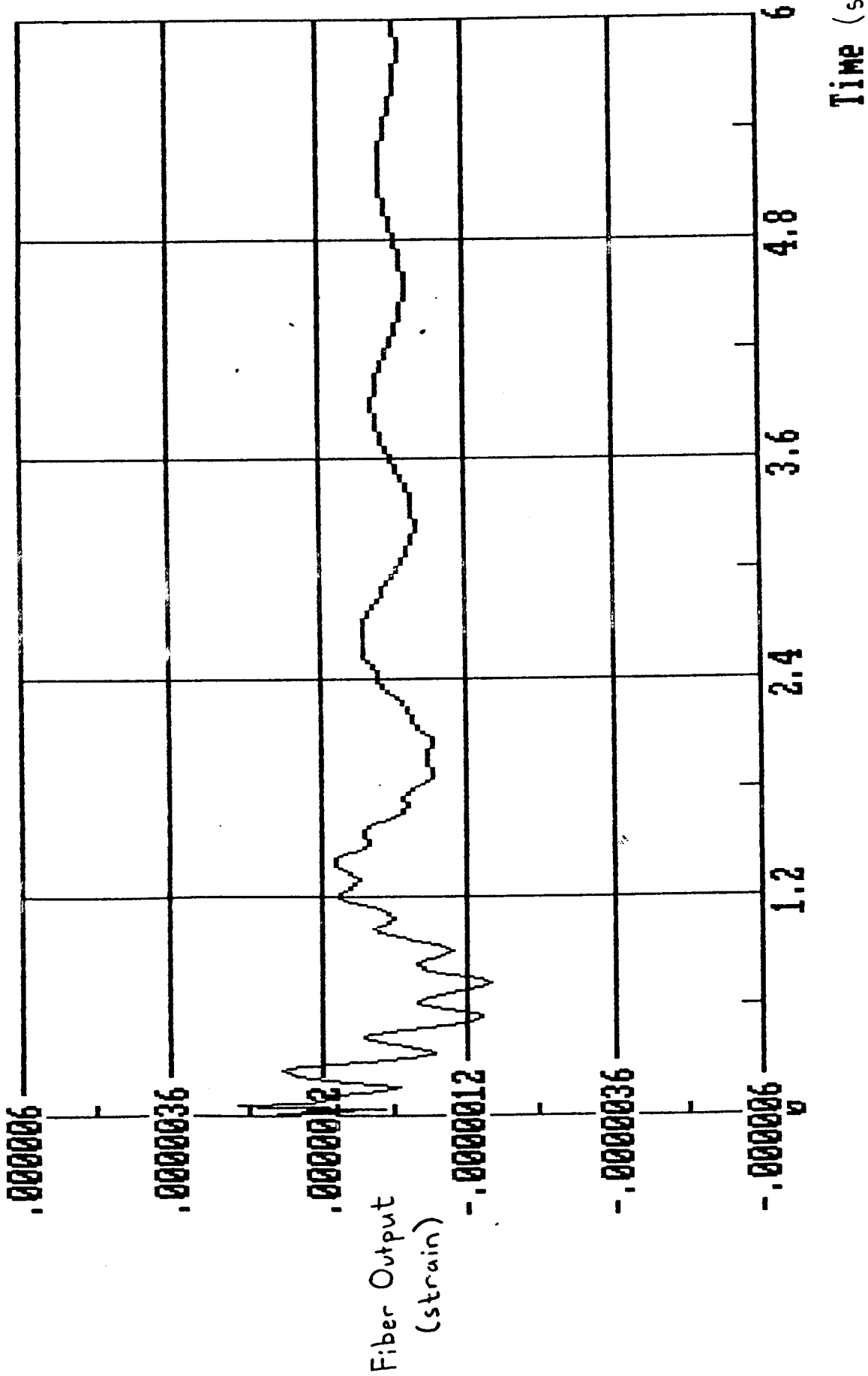


Figure 9: Optical Fiber Sensor
Time Response of Compensated
System

simulation software. Final designs will then be constructed on a breadboard and tested on the flexible beam setup. A performance criteria for comparing the two control system designs will be developed. Numerical experiments will be performed to check the robustness of the respective designs.

ORIGINAL PAGE IS
OF POOR QUALITY

4. SENSOR DEVELOPMENT

The fiber optic sensor has very interesting properties in terms of control systems. The sensors presently employed in control systems feedback information from one point. This information is weighted with a gain and summed with signals from other sensors. This composite signal can then be used to drive the input to the system. Through dynamic analysis it is possible to determine the number of sensors and the associated gains required to tailor the systems performance to within specific criteria.

The optical sensor, however, is a distributed sensor. It measures the integral of strain along its path. The output of the optical fiber is given by:

$$I_f(t) = K_o \int_0^l g(x) \epsilon(x,t) dx$$

Where $\epsilon(x,t)$ is the time varying strain along the beam and $g(x)$ is a weighting factor. This integral can be viewed as the sum of an infinite number of point strain sensors. The weighting factor on these theoretical point sensors is related to the sensitivity of the fiber to strain at each point. If the fiber's sensitivity were modified along its path it would be possible to specify the gain on strain sensed at each point. This concept is called

distributed gain feedback. The advantage of distributed gain feedback is that a control law can be incorporated directly into the sensor, and the sensor's signal contains information which would require many point sensors.

Methods of weighting the fiber's sensitivity have been discussed. The simplest method would involve altering the strength of the bonding material which attaches the fiber to the beam. This could be done by using different types of epoxy to secure the fiber at different points along the beam. A more sophisticated approach would involving varying the thickness of the fiber's coating along the length of the fiber. This could be done in a drawing process using a controlled aperture. The fiber would be less sensitive to strain in those areas where the coating was thick. By specifying the coating thickness along the fiber, a specific distributed gain control law could be implemented.

The design of a distributed feedback gain presents new and challenging problems. These issues are currently being independently investigated, motivated by the experimental work conducted under this project.

REFERENCES

1. B.Y. Kim, J.N. Blake, S.Y. Huang, and H.J. Shaw; "Use of highly elliptical core fibers for two-mode fiber devices", Optics Letters, Vol 12, No. 9, September 1987.
2. J.N. Blake, S.Y. Huang, B.Y. Kim, and H.J. Shaw; "Strain effects on highly elliptical core two-mode fibers", Optics Letters, Vol 12, No. 9, September 1987.
3. K.D. Bennett, J.C. McKeeman, and R.G. May; "Full Field Analysis of Modal Domain Sensor Signals for Structural Control", Proceedings from SPIE International Symposium and Exhibition on Fiber Optics, Optoelectronics and Laser Applications, (Boston MA), September 1988

APPENDIX A

PRELIMINARY REPORT
ON OPTICAL FIBER SENSORS AND SIGNAL PROCESSING
FOR INTELLIGENT STRUCTURE MONITORING

NASA GRANT NAG-1-895

AUGUST 1988

Prepared for Dr. Robert Rogowski
NASA Langley Research Center
Hampton VA 23665

Prepared by Daniel Thomas
Dave Cox
FEORC Virginia Tech
Blacksburg VA 24061

PRELIMINARY REPORT
ON
OPTICAL FIBER SENSORS AND SIGNAL PROCESSING
FOR INTELLIGENT STRUCTURE MONITORING

NASA GRANT

AUGUST 1988

Prepared for: Dr. Robert Rogowski
NASA Langley Research Center
Hampton, VA 23665

Prepared by: Daniel Thomas
David Cox

SUMMARY

The purpose of this report is to give initial progress and outline future plans in the research being carried out for NASA by the Fiber and Electro-Optics Research Center at Virginia Tech. The main emphasis of this project is on using a modal domain sensor in controlling the vibrations in a flexible slewing beam. To date extensive literary research has been conducted on both the modal domain sensor and the control algorithms required to suppress vibrations in the beam. A preliminary experiment has been performed in which the fiber sensor successfully detected the vibrational modes in a clamped-free beam. The bulk of this report will be broken down into four sections:

- 1) Theory behind modal domain sensing.
- 2) Modeling of beam, motor and sensor dynamics.
- 3) Discussion of preliminary experiment and results.
- 4) Discussion of slewing beam experiment; setup, procedures and expected results.

ORIGINAL PAGE IS
OF POOR QUALITY

MODAL DOMAIN SENSING THEORY

To understand the modal domain sensor one must first examine the properties of an optical waveguide. When monochromatic light is launched into a fiber its power is distributed over all of the possible modes. A mode is a solution to Maxwell's equations and is subject to boundary conditions imposed by the physical system. These modes have different phase velocities, which depend upon the waveguide parameters. It is this characteristic which makes modal domain sensing possible. Since stress will alter the fiber's parameters, i.e. length and index of refraction, the resulting phase shift should produce a predictable interference pattern. This pattern can be analyzed to yield the original stress induced in the fiber.

To obtain a practical sensor arrangement the fiber should only support two modes. This is accomplished by using a 633 nm Helium-Neon laser to excite fiber which is designed to support only one mode at 820 nm. The normalized frequency, or V number, for such an arrangement is 3.11. Figure 1 shows the mode cut off curves, for linearly polarized modes, as a function of V number and the normalized propagation constant. It can be seen from this figure that a V number of 3.11 is above the two mode cut off point, but is below that required for three mode propagation. The far field intensity pattern from these modes is a two lobe pattern in which the lobes exchange power as the intermodal phase difference varies. This pattern has been predicted from first principles, and these derivations can be found in Appendix A.

In order to quantify the effects of strain on the intensity pattern the effects of strain on the phase of each mode must be described. Strain along the axis of a fiber causes a shift in the index of refraction and a slight increase in length. The effective phase shift is given by

$$\Delta\phi = \frac{\partial\phi}{\partial n} \Delta n + \frac{\partial\phi}{\partial z} \Delta z \quad (1)$$

The phase of a wave is given by

$$\phi = \beta z + \psi \quad (2)$$

Where β is the propagation constant for a particular mode, and ψ is a random phase term.

Expression (1) can be reduced to

$$\Delta\phi = z \frac{\partial\beta}{\partial n} \Delta n + \beta \Delta z \quad (3)$$

It can be further shown that [1]

$$\frac{\partial \beta}{\partial n} = \frac{\beta}{n} \quad (4)$$

and

$$\Delta n = -\epsilon_z \left\{ \frac{n^3}{2} (1 - \nu) p_{12} - \nu p_{11} \right\} \quad (5)$$

Where:

p_{11} and p_{12} are photoelastic constants
 ν is Poisson's ratio
 ϵ_z is induced strain
 and n is the index of refraction of the core.

By letting σ equal the constant term in brackets in equation (5), and noting that

$$\Delta z = z \epsilon_z \quad (6)$$

The phase change of a mode due to axial strain can be written

$$\Delta \phi = \epsilon_z z \beta (1 - \sigma) \quad (7)$$

This, however, represents an absolute phase shift of one mode. Interference will occur due to the relative phase shift between two modes. This quantity is given by

$$\Delta \phi_{12} = \Delta \phi_1 - \Delta \phi_2 = \epsilon_z z (\beta_1 - \beta_2) (1 - \sigma) \quad (8)$$

This phase shift is not measured directly. Instead the effect of phase shift on the intensity of the far field pattern is monitored. The output pattern is spatially filtered, allowing the photodetector to see only a small section of one lobe. If the initial pattern consists of two lobes of equal intensity and the aperture is placed at the peak of one lobe the intensity is given by [A1]

$$I = I_p \cos^2 \left\{ \frac{\Delta \beta (1 - \sigma) \epsilon_z z}{2} - \frac{\pi}{4} \right\} \quad (9)$$

For small changes in strain the intensity variation can be approximated by the linear expression

$$\Delta I = \frac{I_p}{2}(1 - \sigma)\Delta\beta\Delta\epsilon_z z \quad (10)$$

This expression is an approximation which will yield results with less than 10% error, for variations in phase of plus or minus 35 degrees. This puts a maximum strain limit on the fiber sensor, after which it becomes nonlinear and eventually cyclic.

ORIGINAL PAGE IS
OF POOR QUALITY

BEAM, MOTOR, AND SENSOR DYNAMICS

The flexible beam dynamics will now be developed. The coordinate system that will be used is shown in Figure 2. The linear equations of motion and boundary conditions for a flexible beam with torque actuation at the hub, obtained from Hamilton's Extended Principle, are as follows [B]

$$EI \frac{\partial^4 y}{\partial x^4} + \rho \frac{\partial^2 y}{\partial x^2} + \rho x \frac{\partial^2 \theta}{\partial t^2} = f(x, t) , \quad 0 \leq x \leq l , \quad t > 0 \quad (11)$$

$$(J_h + J_b) \frac{\partial^2 \theta}{\partial t^2} + \rho \int_0^l x \frac{\partial^2 y}{\partial t^2} dx = \tau_l(t) \quad (12)$$

$$y(0, t) = 0 , \quad \frac{\partial y}{\partial x}(0, t) = 0 \quad (13)$$

$$\frac{\partial^2 y}{\partial x^2}(l, t) = 0 , \quad \frac{\partial^3 y}{\partial x^3}(l, t) = 0 \quad (14)$$

where

- E = Young's modulus
- I = area moment of inertia about the bending axis
- $y(x, t)$ = local transverse displacement
- $\theta(t)$ = global angle of rotation
- τ_l = torque applied to the beam
- J_b = beam mass moment of inertia about the hub
- J_h = hub mass moment of inertia
- l = length of the beam
- ρ = beam mass per unit length

If it is assumed that the rigid body motion of the beam is fixed to an inertial frame of reference, then the global angle of rotation is constant. By setting all external forces to zero and assuming that the global angle of rotation is zero, the following partial differential equation results.

$$EI \frac{\partial^4 y}{\partial x^4} + \rho \frac{\partial^2 y}{\partial x^2} = 0 , \quad 0 \leq x \leq l , \quad t > 0 \quad (15)$$

The method of separation of variables will be used to solve this differential equation. The assumed solution to equation (5) is an infinite sum of the product of spatially dependent functions called mode shapes and time dependent functions called modes.

ORIGINAL PAGE IS
OF POOR QUALITY

$$y(x, t) = \sum_{n=1}^{\infty} \psi_n(x) r_n(t) \quad (16)$$

where

$\psi_n(x)$ = mode shapes

$r_n(t)$ = modes, mode shapes

After substituting equation (16) into equation (15) and separating the variables, we get.

$$\frac{EI}{\psi_n(x)} \frac{\partial^4 \psi_n(x)}{\partial x^4} = - \frac{\rho}{r_n(t)} \frac{\partial^2 r_n(t)}{\partial t^2} = -B_n^4 \quad (17)$$

For this equation to be valid, both sides have to be equal for all x and t , thus they must be equal to a constant. The constant will be referred to as B_n^4 . This yields the following differential equation.

$$\frac{d^4 \psi_n(x)}{dx^4} + \frac{B_n^4 \psi_n(x)}{EI} = 0 \quad (18)$$

$$\psi_n(0) = 0 \quad , \quad \frac{d\psi_n}{dx}(0) = 0 \quad (19)$$

$$\frac{d^2 \psi_n}{dx^2}(l) = 0 \quad , \quad \frac{d^3 \psi_n}{dx^3}(l) = 0 \quad (20)$$

Solving differential equation (18) subject to boundary conditions (19) and (20) yields

$$\psi_n(x) = C_n \{ \cosh(B_n x) - \cos(B_n x) - \epsilon_n [\sinh(B_n x) - \sin(B_n x)] \} \quad (21)$$

where

$$\epsilon_n = \frac{\cos(B_n l) + \cosh(B_n l)}{\sin(B_n l) + \sinh(B_n l)} \quad (22)$$

and the real numbers B_n satisfy the characteristic equation

$$1 + \cos(B_n l) \cosh(B_n l) = 0 \quad , \quad n = 1, 2, \dots \quad (23)$$

Now that the expression for mode shapes has been solved for, half of the solution to $y(x, t)$ has been obtained. The other half of the solution is the time response of the system. The time response is obtained by setting up the differential equations in terms of $r_n(t)$. Substituting equation (16) into equations (11) and (12) yields

$$EI \sum_{n=1}^N \frac{d^4 \psi_n(x)}{dx^4} r_n(t) + \rho \sum_{n=1}^N \psi_n(x) \frac{d^2 r_n(t)}{dt^2} + \rho x \frac{d^2 \theta(t)}{dt^2} = f_d(x) f(t) \quad (24)$$

$$(J_b + J_h) \frac{d^2 \theta(t)}{dt^2} + \rho \int_0^l x \psi_n(x) \frac{d^2 r_n(t)}{dt^2} dx = \tau_l(t) \quad (25)$$

where $f(x,t)$ is expressed as a product of a spatially dependent function and a time dependent function. The infinite sum was also changed to a finite sum. This was done because it is practical to think of a finite order system. The order of this system will be determined at a later time.

Equation (25) accounts for one solution and equation (24) accounts for N solutions. Thus, to obtain the required $N+1$ equations for solving this system, it is convenient to multiply both sides of equation (24) by $\psi_m(x)$ and integrate over the length of the beam. This yields

$$\sum_{n=1}^N M_{rr}^{nm} \frac{d^2 r_n(t)}{dt^2} + \sum_{n=1}^N K_{rr}^{nm} r_n(t) + M_{r\theta}^m \frac{d^2 \theta(t)}{dt^2} = B_m f(t) \quad , \quad 0 \leq m \leq N \quad (26)$$

where

$$M_{rr}^{nm} = \rho \int_0^l \psi_n(x) \psi_m(x) dx = \rho l \delta_{nm} \quad (27)$$

$$M_{r\theta}^m = \rho \int_0^l x \psi_m(x) dx \quad (28)$$

$$K_{rr}^{nm} = EI \int_0^l \psi_m(x) \frac{d^4 \psi_n(x)}{dx^4} dx = EIl B_n^4 \delta_{nm} \quad (29)$$

$$B_m = \int_0^l \psi_m(x) f_d(x) dx \quad (30)$$

and δ_{nm} is the Kronecker delta function. The simplifications of equations (27) and (29) come from the orthogonality property of mode shapes. Equation (29) is also simplified by the substitution of equation (17). Using this notation, equation (25) can be written as

$$(J_b + J_h) \frac{d^2 \theta(t)}{dt^2} + \sum_{n=1}^N M_{r\theta}^n \frac{d^2 r_n(t)}{dt^2} = \tau_l(t) \quad (31)$$

where

$$M_{r\theta}^n = \rho \int_0^l x \psi_n(x) dx$$

which is also the transpose of equation (28).

Equations (26) and (31) are now put into vector matrix form. Before this is done, a finite dimension column vector r will be defined as

$$r = \begin{pmatrix} r_1 \\ r_2 \\ \vdots \\ r_N \end{pmatrix} \quad (32)$$

The vector matrix form of the flexible beam dynamics is thus

$$\begin{pmatrix} J_r + J_h & M_{r\theta}^T \\ M_{r\theta} & M_{rr} \end{pmatrix} \begin{pmatrix} \ddot{\theta} \\ \dot{r} \end{pmatrix} + \begin{pmatrix} 0 & 0 \\ 0 & K_{rr} \end{pmatrix} \begin{pmatrix} \theta \\ r \end{pmatrix} = \begin{pmatrix} 1 & 0 \\ 0 & B \end{pmatrix} \begin{pmatrix} \tau_L(t) \\ f(t) \end{pmatrix} \quad (33)$$

The model will now be developed for the DC motor dynamics. The model that is used here is a separately excited DC motor model.[2] The circuit diagram is shown in Figure 3. It is assumed that the motor will be operated in the linear region and that the field voltage $e_f(t)$ is applied long enough so the field current $i_f(t)$ is constant. With these assumptions, the following linear equations apply.

$$\phi(t) = K_f i_f(t) = K_f I_f = \text{constant} \quad (34)$$

$$\tau_m(t) = K_m \phi(t) i_a(t) = K_m K_f I_f i_a(t) \quad (35)$$

By letting

$$K_i = K_m K_f I_f$$

yields the following

$$\tau_m(t) = K_i i_a(t) \quad (36)$$

The differential equations that describe the motion of the D.C. motor are given as

$$\frac{di_a(t)}{dt} = -\frac{R_a}{L_a} i_a(t) + \frac{1}{L_a} e_a(t) - \frac{1}{L_a} e_b(t) \quad (37)$$

$$\frac{d\omega_m(t)}{dt} = \frac{1}{J} \tau_m(t) - \frac{1}{J} \tau_L(t) - \frac{B_m}{J} \omega_m(t) \quad (38)$$

where

$$e_b(t) = K_b \omega_m(t) \quad (39)$$

and substituting equation (39) into equation (37) yields

$$\frac{di_a(t)}{dt} = -\frac{R_a}{L_a} i_a(t) - \frac{K_b}{L_a} \omega_m(t) + \frac{1}{L_a} e_a(t) \quad (40)$$

and substituting equation (36) into equation (38) yields

$$\frac{d\omega_m(t)}{dt} = \frac{K_i}{J} i_a(t) - \frac{B_r}{J} \omega_m(t) - \frac{1}{J} \tau_l(t) \quad (41)$$

The state variables of the system are defined as $i_a(t)$, $\omega_m(t)$, and $\theta_m(t)$. The following are the state equations in state space form.

$$\begin{pmatrix} \frac{di_a(t)}{dt} \\ \frac{d\omega_m(t)}{dt} \\ \frac{d\theta_m(t)}{dt} \end{pmatrix} = \begin{pmatrix} -\frac{R_a}{L_a} & -\frac{K_b}{L_a} & 0 \\ \frac{K_i}{J} & -\frac{B_m}{J} & 0 \\ 0 & 1 & 0 \end{pmatrix} \begin{pmatrix} i_a(t) \\ \omega_m(t) \\ \theta_m(t) \end{pmatrix} + \begin{pmatrix} \frac{1}{L_a} \\ 0 \\ 0 \end{pmatrix} e_a(t) - \begin{pmatrix} 0 \\ \frac{1}{J} \\ 0 \end{pmatrix} \tau_l(t) \quad (42)$$

The block diagram representation of the D.C. motor is shown in Figure 4. The following is the transfer function between the motor velocity and the input voltage.

$$\frac{\Omega_m(s)}{E_a(s)} = \frac{K_i}{L_a J s^2 + (R_a J + B_m L_a) s + K_b K_i + R_a B_m} \quad (43)$$

Since typically $L_a \ll R_a$ and $B_m \approx 0$, the following simplification of the transfer function results.

$$\frac{\Omega_m(s)}{E_a(s)} = \frac{K_i K_v}{R_a J s + K_b K_i} \quad (44)$$

where K_v is the tachometer constant and will be determined experimentally. Equation (44) will be tested against the frequency response of the motor.

It is now desired to integrate the motor dynamics together with the flexible beam dynamics. From equation (41) and the motor block diagram in Figure 4, the torque supplied to the beam is given by

$$\tau_l(t) = \frac{K_i}{R_a} e_a(t) - J \ddot{\theta} - \left(B_m + \frac{K_i K_b}{R_a} \right) \dot{\theta} \quad (45)$$

Substituting equation (45) into equation (33) for $\tau_l(t)$ yields the following state equations for the beam and motor dynamics.

$$\begin{pmatrix} M_{\theta\theta} & M_{r\theta}^T \\ M_{r\theta} & M_{rr} \end{pmatrix} \begin{pmatrix} \ddot{\theta} \\ \ddot{r} \end{pmatrix} + \begin{pmatrix} D_{\theta\theta} & 0 \\ 0 & 0 \end{pmatrix} \begin{pmatrix} \dot{\theta} \\ \dot{r} \end{pmatrix} + \begin{pmatrix} 0 & 0 \\ 0 & K_{rr} \end{pmatrix} \begin{pmatrix} \theta \\ r \end{pmatrix} = \begin{pmatrix} \frac{K_i}{R_a} \\ 0 \end{pmatrix} e_a(t) \quad (46)$$

or equivalently,

$$M \begin{pmatrix} \ddot{\theta} \\ \ddot{r} \end{pmatrix} + D \begin{pmatrix} \dot{\theta} \\ \dot{r} \end{pmatrix} + K \begin{pmatrix} \theta \\ r \end{pmatrix} = Q e_a(t) \quad (47)$$

where

$$M_{\theta\theta} = J_b + J_h + J \quad (48)$$

$$D_{\theta\theta} = B_m + \frac{K_i K_b}{R_a} \quad (49)$$

The fiber optic sensor will measure the integral of the strain on the flexible beam. Denoting the output of the optical fiber by $I_f(t)$, then

$$I_f(t) = K_o \int_0^l \epsilon(x, t) dx \quad (50)$$

where

$\epsilon(x, t)$ = strain of the flexible beam
 K_o = proportionality constant

From [B] we have

$$I_f(t) = C_I \begin{pmatrix} \theta \\ r \end{pmatrix} \quad (51)$$

where

$$C_{IN} = (0 \quad C_{I1} \quad C_{I2} \quad \dots) \quad (52)$$

with

$$C_{IN} = \frac{\partial \psi_n(x)}{\partial x} \text{ evaluated at } x=l \quad (53)$$

The state space model of the system will now be developed. The following state variable is chosen.

$$x = \begin{pmatrix} \theta \\ r \\ \dot{\theta} \\ \dot{r} \end{pmatrix} \quad (54)$$

which yields the state space model

$$\dot{x} = Ax + Be_a \quad (55)$$

$$y = Cx$$

where

$$A = \begin{pmatrix} 0 & I \\ -M^{-1}K & -M^{-1}K \end{pmatrix} \quad (56)$$

$$B = \begin{pmatrix} 0 \\ M^{-1}Q \end{pmatrix} \quad (57)$$

$$C = \begin{pmatrix} 1 & 0 & \dots & 0 \\ C_{11} & C_{12} & \dots & C_{1N} \\ C_{21} & C_{22} & \dots & C_{2N} \\ \dots & \dots & \dots & \dots \\ C_{I1} & C_{I2} & \dots & C_{I\epsilon} \end{pmatrix} \quad (58)$$

and M, D, K, and Q are the coefficient matrices in equation (47).

PRELIMINARY EXPERIMENT

The purpose of this preliminary experiment was to test the sensors ability to sense dynamic strain, and to characterize noise so that simulations could yield more realistic results. The fiber was fixed to a beam of sheet metal in a looped pattern using epoxy. This beam was then clamped at one end and suspended vertically as shown in Figure 5. This configuration minimized strain effects due to the beam's own weight and allowed vibrations to occur with little damping. A photodetector with a pinhole aperture was positioned to monitor the peak of one lobe of the far field pattern. The best signal was obtained when the photodetector was left unbiased and connected directly to the oscilloscope.

The beam was excited by simply displacing its bottom end and allowing it to swing back and forth freely. After allowing initial transients to die out the photodetector signal was stored on a digital oscilloscope (LeCroy 9400A). The signal was then processed, via a FFT algorithm, to obtain frequency information. Figure 6 is the photodetector signal recorded a few seconds after the beam was excited. Figure 7 is the frequency spectrum of this signal, from D.C. to 25 Hz. Frequency peaks occur at 1.8 Hz and 11.3 Hz, corresponding to the first two vibrational modes of the beam. Theory predicts that the second vibrational mode of a clamped-free beam should occur at a frequency of 6.267 times the fundamental mode.[3] The ratio of experimentally determined frequencies is 6.27, which is in excellent agreement with theory.

A second independent test was performed to verify the fundamental frequency of the beam. A laser was directed across the bottom of the beam intersecting its thin axis. On the other side of the beam a photodetector was positioned to receive the laser light. This arrangement is shown in Figure 8. When the beam was excited, it cut the lasers path at the bottom of its swing. This produced two interceptions of the laser beam over each cycle of vibration. The spacing of these spikes in time was very consistent, and thus gave an accurate measurement of the beam's fundamental frequency. The fundamental frequency as measured from this test was 1.84 Hz. This agrees with the results from the modal domain sensor and confirms its ability to sense dynamic strain.

The main problem discovered in this test was one of modal stability. The fiber only supports two linearly polarized modes, however, the second mode has four unpolarized degeneracies. If the launching conditions are not perfect, or if the fiber is perturbed in some way, power may be coupled into these unwanted modes. This creates a pattern which will shift upward or downward from the two lobe pattern as the fiber undergoes stress. This instability makes it difficult to characterize the fiber sensor, and hinders its use in practical applications. A possible solution to this problem lies in the use of optical fiber with a highly elliptical core. The elliptical core has been shown to eliminate these degeneracies and stabilize the two mode fiber waveguide.[4] A sample of elliptical core fiber has been ordered, and if experimentation verifies its properties it will be used on future modal domain sensing experiments.

SLEWING BEAM EXPERIMENT

We will now turn to the proposed slewing beam experiment that will be performed here at Virginia Tech. The test setup is instrumented as shown in Figure 9. The flexible beam to be used is made of steel with dimensions and parameters as displayed in Table 1.

l	0.76 m
h	0.076 m
W	0.00081 m
E	206.85 GPa
$Mass$	0.3662 Kg
ρ	0.4818 Kg/m
$J_b + J_h$	0.0706 Kg m ²

TABLE 1
Beam Dimensions and Parameters

The flexible beam is cantilevered and forced to rotate in the horizontal plane by the electric DC motor. The instrumentation in this setup consists of:

An optical fiber, laser, and optical detector for sensing.

A potentiometer and tachometer, to measure the angle of rotation and motor shaft velocity, respectively.

A function generator for the DC motor input

Instrumentation for the beam controller that will be determined later.

It should be noted that the tachometer is built into the motor. There will also be two limit switches to limit the angle of rotation to avoid system damage. The fiber is to be looped around on side of the flexible beam and attached with epoxy.

An important aspect of this experiment is the characterization of the sensors performance. We wish to demonstrate a system which will not only perform well, but also one which will agree with theoretical predications. Therefore, the first stage in this experiment will be to verify the motors parameters. This will be done by determining the motors open loop response to low frequency AC excitation. The motor will also be tested for maximum operating voltage and linearity of response. Once these parameters are known a control loop will be designed to improve the motors ability to track a step input. This step response will be tested to ensure that it can be approximated as an ideal step input to the beam.

The second stage of this experiment will be to verify the beam parameters. This will be done by applying a step input, but no vibrational control to the motor. The fiber sensor or the strain gauges will then be used to sense the beams vibrational pattern. If this pattern does not meet with theoretical predictions then the beam parameters will be reevaluated, and a more accurate model of beam dynamics will be constructed.

Once the parameters of the experimental system have been verified they will be used to generate a simulation program. This simulation program will consider noise inputs from the sensor, as well as nonlinear effects from the motor. Using this program the suggested control law will be tested and refined. Only when an adequate control law has been developed, one which is robust and displays noise immunity, will the actual experiment be conducted. The control will be performed by an analog computer, or by digital signal processing chips depending upon our needs. Hopefully this experiment will yield results consistent with theory, and will demonstrate the use of fiber as a real time sensor of dynamic strain.

REFERENCES

1. C. D. Butter and G. B. Hocker; "Fiber Optics Strain Guage", Applied Optics, Vol. 17, No. 18, 15 September 1978.
2. B. C. Kuo, Automatic Control Systems, Prentice Hall Inc., Englewood Cliffs, N.J., Ch. 4, 1982
3. W. T. Thomson, Theory of Vibrations with Applications, Englewood Cliffs N.J., Appendix D, 1972
4. B.Y. Kim, J. N. Blake, S. Y. Huang, and H. J. Shaw; "Use of highly elliptical core fibers for two-mode fiber devices", Optics Letters, Vol. 12, No. 9, September 1987

ORIGINAL PAGE IS
OF POOR QUALITY

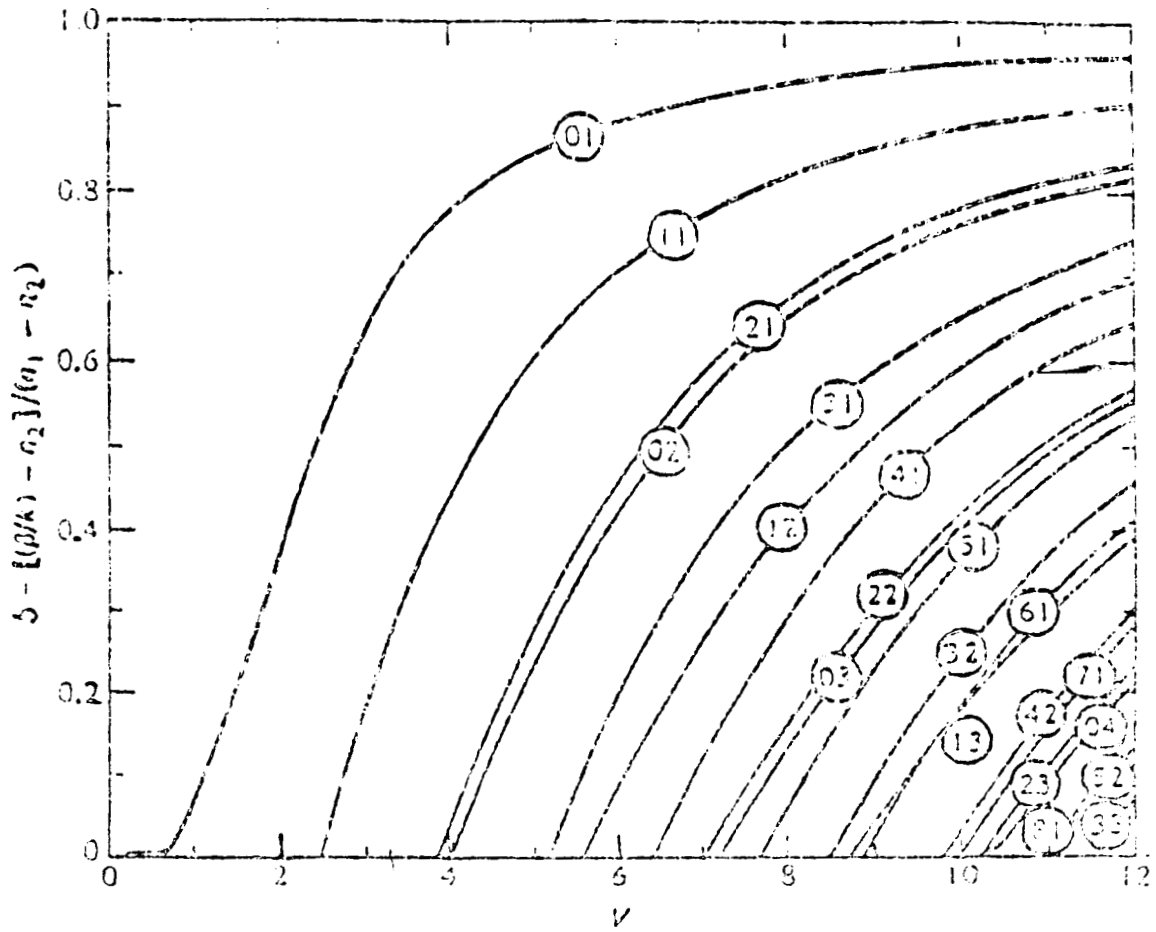


FIGURE 1

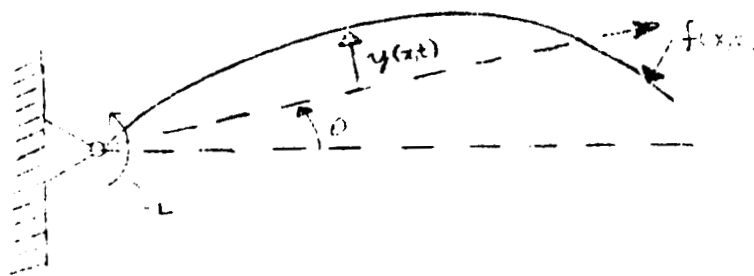
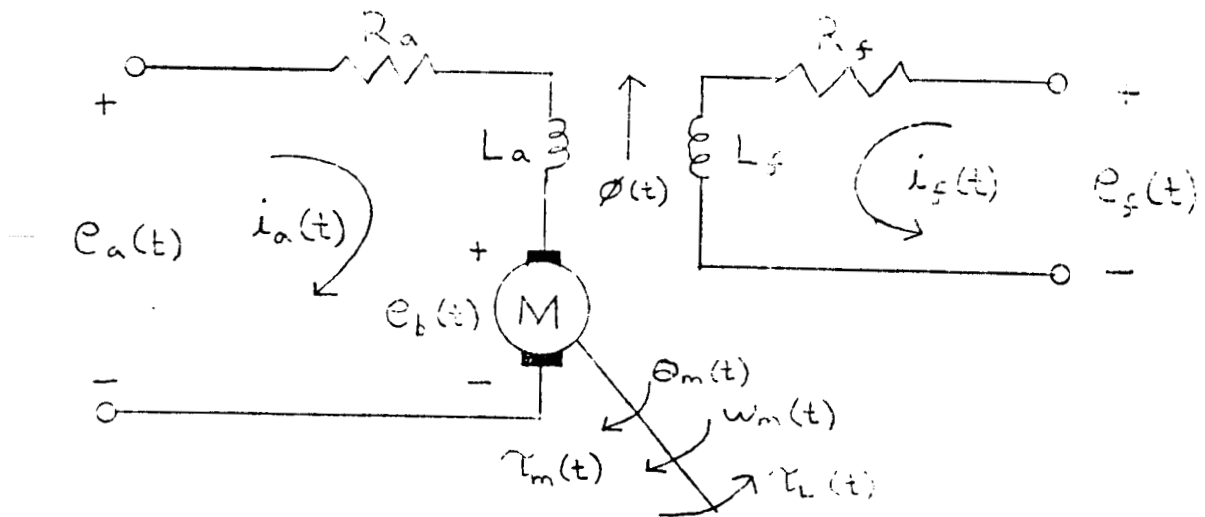


FIGURE 2 BEAM MODEL COORDINATE
SYSTEM

ORIGINAL PAGE IS
OF POOR QUALITY



- K_i = torque constant = $0.309574 \text{ (N}\cdot\text{m/A)}$
 K_b = back emf constant = $0.309397 \text{ (V}\cdot\text{s/rad)}$
 L_a = armature inductance = 2.8 mH
 R_a = armature resistance = 1.5Ω
 R_f = field resistance
 J_m = rotor inertia of motor = $2.6 \times 10^{-4} \text{ kg}\cdot\text{m}^2$
 J_s = inertia of attached shaft = $1.52 \times 10^{-4} \text{ kg}\cdot\text{m}^2$
 J = inertia of rotor and shaft = $4.12 \times 10^{-4} \text{ kg}\cdot\text{m}^2$
 $e_a(t)$ = armature voltage
 $e_f(t)$ = field voltage
 $e_b(t)$ = back emf
 L_f = field inductance
 $i_a(t)$ = armature current
 $i_f(t)$ = field current
 $\phi(t)$ = magnetic flux
 $\tau_m(t)$ = torque developed by motor
 $\tau_L(t)$ = load torque
 B_m = viscous frictional coefficient
 $\theta_m(t)$ = rotor angular displacement
 $\omega_m(t)$ = rotor angular velocity

FIGURE 3 SEPARATELY EXCITED DC MOTOR
DIAGRAM AND PARAMETERS

ORIGINAL PAGE IS
OF POOR QUALITY

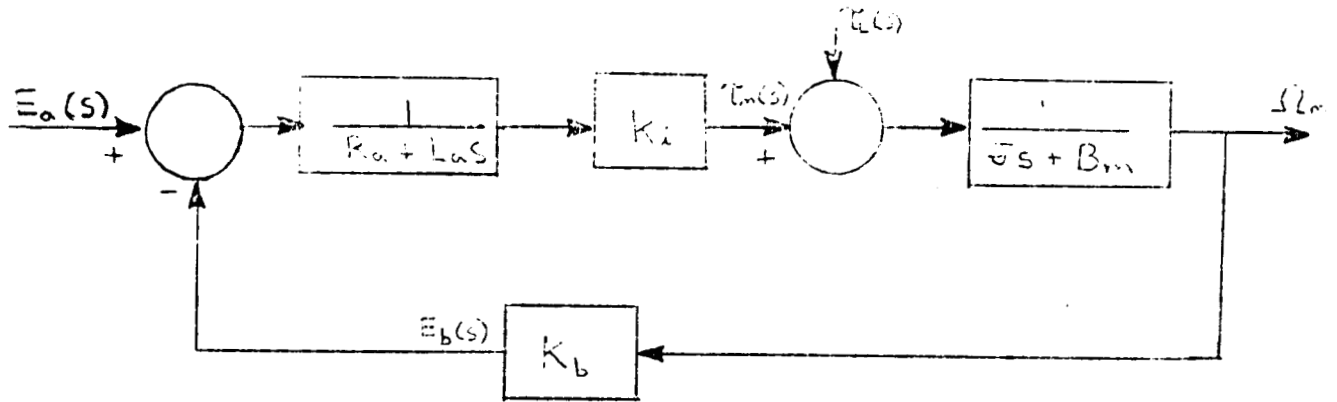


FIGURE 4 BLOCK DIAGRAM OF DC MOTOR

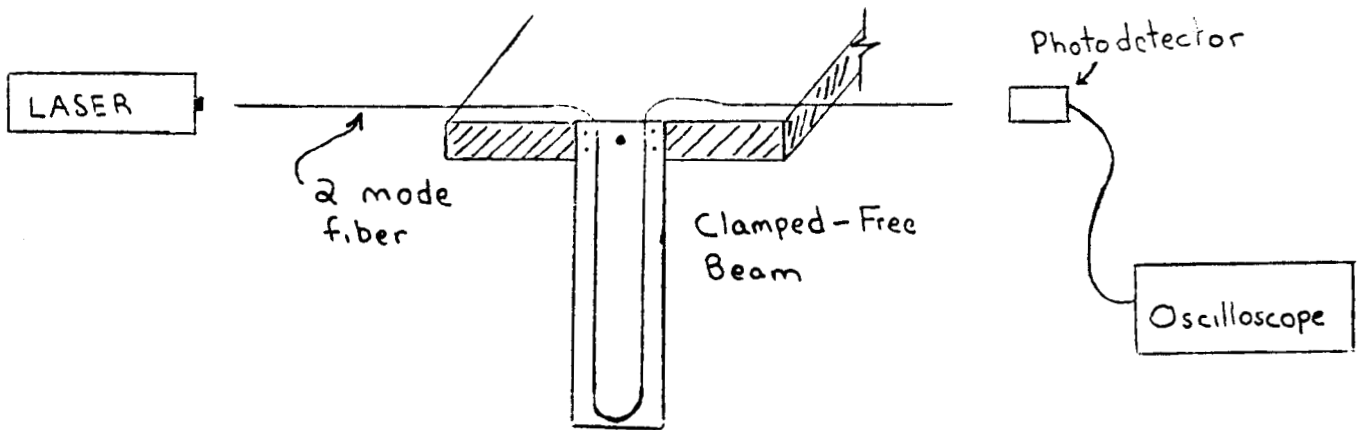
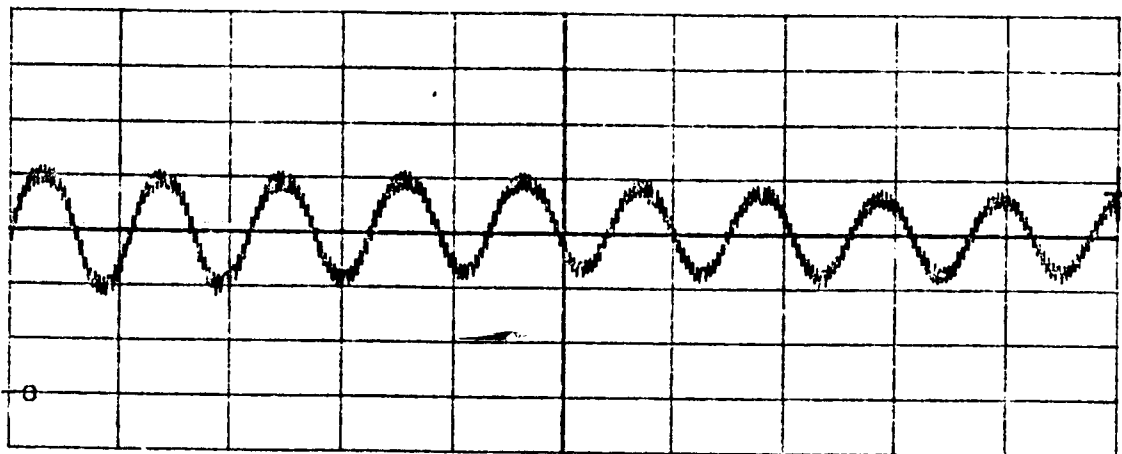


FIGURE 5 DYNAMIC SENSOR
EXPERIMENT

ORIGINAL PAGE IS
OF POOR QUALITY



.5 Sec/ Div

FIGURE 6 Photodetector Signal

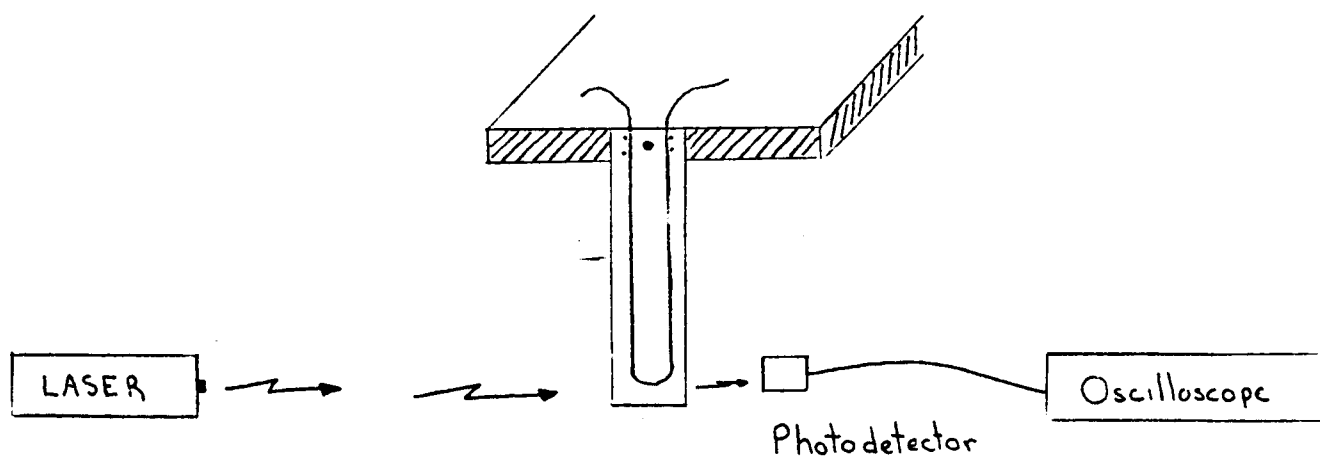
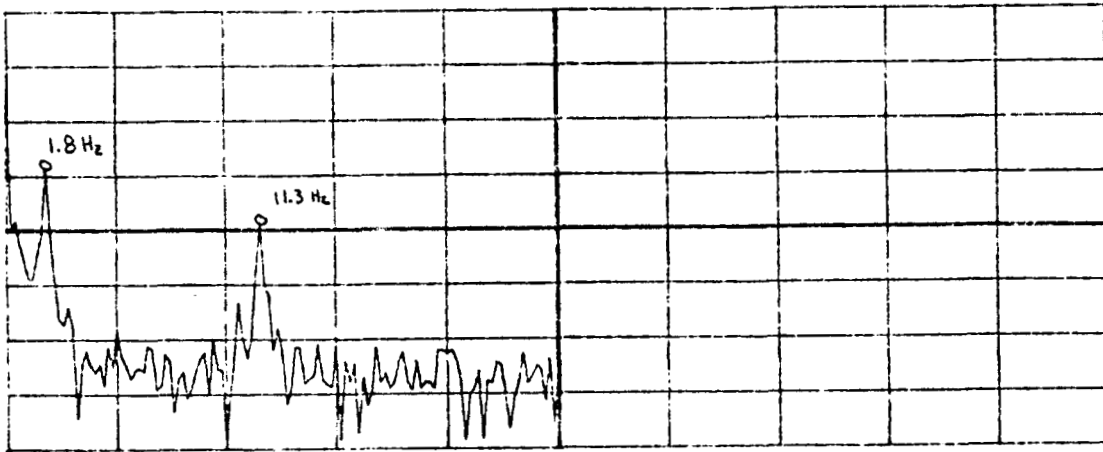


FIGURE 7 Beam Frequency Experiment



5 Hz/Div

FIGURE 8 Frequency Spectrum

ORIGINAL PAGE IS
OF POOR QUALITY

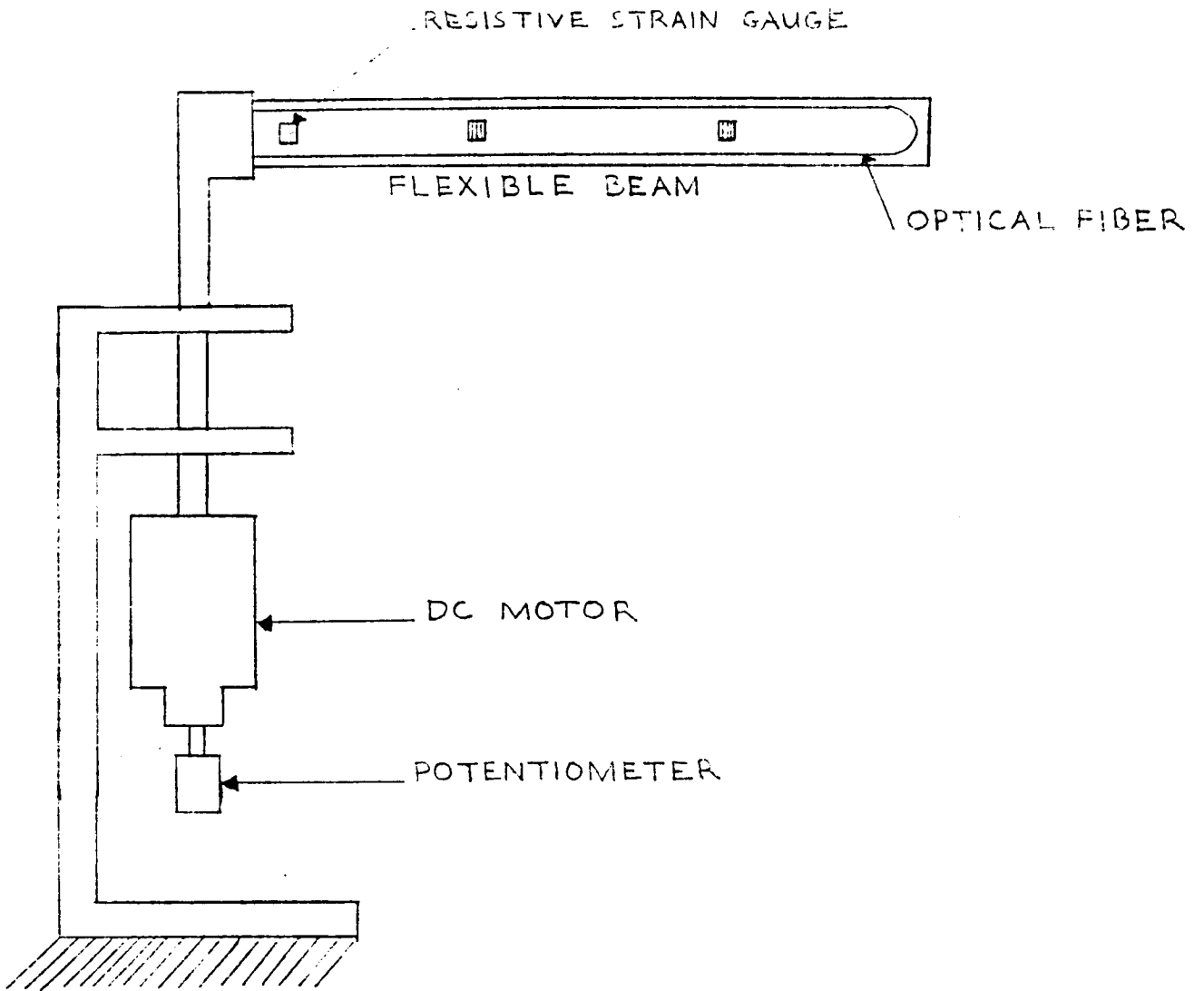


FIGURE 9 FLEXIBLE SLEWING BEAM